

# THE EFFECT OF SPECIMEN SIZE ON WETTING-INDUCED STRESS IN SELF-TAPPING SCREWS IN STEEL-TO-WOOD CONNECTIONS

Jintao Zhang<sup>1</sup>, Lina Zhou<sup>2</sup>, Chun Ni<sup>3</sup>

**ABSTRACT:** When a steel-to-wood connection fabricated with self-tapping screws (STSs) is subjected to wetting exposure, due to the hygroscopic characteristics of wood, tensile stress develops in the STSs. Meanwhile, compressive stress arises in the wood. The wetting-induced stress may lead to the failure of the STS, typically characterized by the fracture of the STS. This type of failure has been attributed to the excessively long STS penetration and/or extensive increases of moisture content in wood. Analytical equations have been derived to predict the STS stress in previous study by the authors. However, in this analytical model of a steel-to-wood connection with single STS, the size of the wood specimen was assumed to be related to the penetration length of STSs or the size of the steel plate, which may play a critical role in the prediction of the wetting-induced stress in both STS and wood. In this study, sensitivity analysis was performed via numerical modelling on 8 mm and 13 mm diameter STS connections with different wood specimen size. Results show that wetting-induced stress in STS increases with the increase of wood specimen size but eventually approaches a constant value when the edge length of wood is larger than the penetration length of STSs.

**KEYWORDS:** size effect, self-tapping screw, wetting-induced stress, numerical modelling.

## 1 – INTRODUCTION

Steel-to-wood connections with self-tapping screws (STSs) are commonly used in modern mass timber construction due to their high load-carrying capacity and ease of installation. However, due to the hygroscopic characteristics of wood, exposure to wetting conditions may cause significant stress in this type of connections and lead to STS breakage. So far, research on moisture content effect on mass timber connections with STSs has been mainly focused on the STS withdrawal behaviour [1–4]. Research on extra stress developed on STSs caused by wetting is limited.

With reported STS breakage in several mass timber projects during construction under wetting, research on wetting-induced stress in STSs in mass timber connections has attracted increasing attention to quantitatively determine the wetting effect on this type of connection [5,6]. Gerstorfer et al. [5] investigated wetting-induced stress in STSs inserted in laminated veneer lumber (LVL) through both tests and numerical analysis. STSs of 6 mm and 8 mm diameters were adopted and inserted at penetration depths of 158 mm (26d) and 238 mm (30d), respectively. In the numerical analysis, 2D models were created and the interaction between STS threads and wood was modeled with ‘hard’ contact. With a moisture content increase of 15%, STS yielding was not observed from the

numerical modelling. This may be due to the specific setting that the screw head was not in direct contact with LVL surface and there was no steel plate between them, so the expansion of LVL under wetting on the screw head side was not constrained and the effective penetration length is equivalent to half of the cases when the LVL surface was blocked by a steel plate on the screw head side. Similarly, Khan et al. [6] developed a 2D axisymmetric model to investigate wetting-induced stress in STSs in both cross laminated timber (CLT) and glulam connections. The interaction between STS and timber element was modelled with cohesive surface, and the mechanical properties of the cohesive surface at different moisture content levels were obtained by fitting to the STS withdrawal test results carried out by Khan et al. [7]. The developed model was able to predict the wetting-induced stress in STS inserted in a cylindrical-shaped wood specimen.

In the above-mentioned studies, the variables in the numerical models were STS diameters and penetration lengths, and none of them conducted a parametric analysis on wood specimen size. However, the cross-sectional dimension of the wood specimen may be a crucial factor, as it controls the overall compressive stiffness and thus affects the magnitude of the wetting-induced stress in STSs.

Analytical equations have been derived by the authors in previous study for prediction of STS stress induced by

<sup>1</sup> Jintao Zhang, PhD student, Department of Civil Engineering, University of Victoria, Victoria, Canada, jintaozhang@uvic.ca.

<sup>2</sup> Lina Zhou, Associate Professor, Department of Civil Engineering, University of Victoria, Victoria, Canada, linazhou@uvic.ca.

<sup>3</sup> Chun Ni, Lead Scientist, Building System, FPInnovations, Vancouver, Canada, Chun.Ni@fpinnovations.ca.

wetting in a steel-to-wood connection. In this analytical model, the size of the wood specimen was assumed to be related to the penetration length of STSs or the size of the steel plate. There is a need to get a better understanding on the sensitivity of this assumption. In this study, the size effect of wood specimen on wetting-induced stress in STSs was investigated with a 3D numerical model of typical steel-to-wood connection developed and verified in previous study by the authors via ABAQUS.

## 2 – NUMERICAL MODELLING ANALYSIS

### 2.1 NUMERICAL MODELLING METHOD

The numerical modelling method adopted in this study is shown in Fig. 1. STS was modelled with a smooth shank with diameter the same as STS core diameter. Ideal elastic-plastic material properties were assumed for STSs. Detailed STS geometries and material properties are summarized in Tabel 1. Orthogonal wood material was assumed for glulam, with wood radial direction aligned with the STS length direction. To consider the moisture content (MC) effect on wood mechanical properties, test results from Gerhards [5] were adopted, i.e., the modulus of elasticity parallel-to-grain and perpendicular-to-grain, and the shear modulus decrease by 1.625%, 2.875% and 2.500%, respectively per 1% MC increase. The Glulam

mechanical properties at 12% MC are listed in Table 2. Based on the measured swelling coefficient of glulam in Khan et al. [7], an average value of the swelling coefficients (0.23%) along wood tangential and radial directions was adopted to account for the random pith location of each laminate. With the assumed orthogonal directions (see Fig. 1(a)), wood swelling along tangential and longitudinal directions would have negligible influence on STS deformation, so swelling coefficient was only assigned to wood radial direction. The interaction between STS and glulam wood was modelled with cohesive surface (a built-in surface-based interaction in ABAQUS). The traction-separation law and coordinates of cohesive surface are shown in Fig. 1. There are three main directions in cohesive surface, two tangential directions ( $t$  and  $s$ ) and one normal direction ( $n$ ). The mechanical properties of the cohesive surface, including stiffness ( $\Gamma$ ), strength ( $t^o$ ) and critical failure energy ( $G_f$ ), need to be defined (see Section 2.2). The moisture transport process was not the primary focus in this study. Therefore, it was assumed that MC changes uniformly throughout the wood during wetting process, requiring only the definition of the initial MC and target MC for the model. Besides, temperature field was utilized to model moisture field in ABAQUS. C3D8 element was adopted for modelling STSs, glulam and steel plates. During the wetting process, the top surface of the steel plate was fixed.

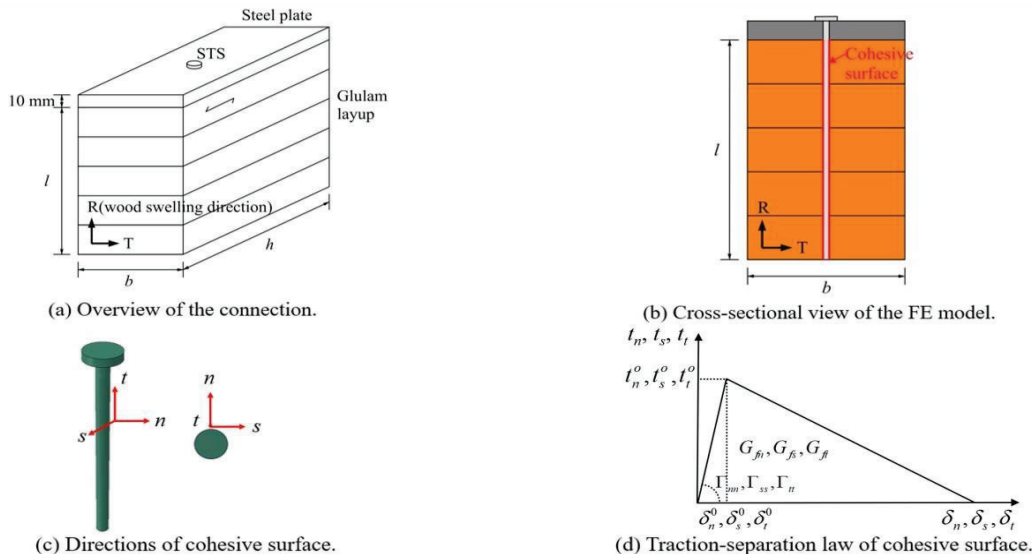


Figure 1: Numerical modelling description.

Table 1: STS geometries and material properties [7].

STS type	Supplier	Thread/root diameter (mm)	Tip length (mm)	Young's modulus (GPa)	Yielding strength (MPa)	Failure strain (%) [8]
ASSY 8	MTC solutions	8/5.2	8	208.2	1192.7	14.3
VGS 13	Rothoblaas	13/8	10	226.6	1093.2	

**Table 2:** Glulam mechanical properties (12% MC) [7,9].

$E_L$ (MPa)	$E_R$ (MPa)	$E_T$ (MPa)	$G_{LR}$ (MPa)	$G_{TL}$ (MPa)	$G_{RT}$ (MPa)	$\nu_{LR}$	$\nu_{LT}$	$\nu_{RT}$
12400	843.2	620	793.6	967.2	86.8	0.390	0.292	0.449

## 2.2 DETERMINATION OF STS-WOOD INTERACTION PROPERTIES

STS withdrawal test results carried out by Khan et al. [7] were utilized to determine the mechanical properties of cohesive surface at a given MC. In their tests [7], before inserting 8 mm and 13 mm diameter STSs into CLT and glulam, mass timber products were conditioned in the environment chamber to reach equilibrium moisture content (EMC), and four EMCs were considered in the test, i.e., 12%, 16%, 21% and fiber saturation point (assumed as 30% in this study). STSs were then inserted into mass timber products to a penetration depth of 10d, followed by STS withdrawal tests. The MC of the test specimens was kept constant throughout the entire test procedure, ensuring no relative movement between the STS and the wood caused by changes of MC. With the obtained withdrawal load-displacement curves, the mechanical parameters can be determined based on the theoretical equations derived by Jensen et al. [10].

$$K_{w,MC} = \pi \cdot d \cdot l \cdot \Gamma_{MC} \cdot \frac{\tanh \omega}{\omega} \quad (1)$$

where  $K_{w,MC}$  is the specimen withdrawal stiffness at a given MC, which can be obtained from withdrawal tests;  $d$  is STS root diameter;  $l$  is STS penetration length;  $\Gamma_{MC}$  is the cohesive surface stiffness at a given MC;  $\omega = \sqrt{\pi \cdot d \cdot \Gamma_{MC} \cdot \beta \cdot l^2}$ , where  $\beta = 1/(A_s \cdot E_s) + 1/(A_w \cdot E_{w,MC})$ ;  $A_s$  is the cross-sectional area of STS core;  $E_s$  is STS modulus of elasticity;  $E_{w,MC}$  is wood radial modulus of elasticity at a given MC;  $A_w$  is the compressive area of

wood under push-pull withdrawal loading condition. In the tests by Khan [7], a steel plate covering the entire cross-sectional area of the wood specimen was used to prevent the movement of the specimen under withdrawal loading.  $A_w$  in this study was assumed as the cross-sectional area of wood element excluding the cross-sectional area of STS. The wood specimen sizes for 8 mm and 13 mm diameter STSs are  $80 \times 160 \times 114$  mm and  $130 \times 260 \times 152$  mm ( $b \times h \times l$  mm in Fig. 1 a)), respectively.

The cohesive surface strength,  $t_{MC}^o$ , at a given MC can be determined by the following equation,

$$t_{MC}^o = \frac{P_{max}}{\pi \cdot d \cdot l} \cdot \frac{\omega}{\tanh \omega} \quad (2)$$

where  $P_{max}$  is the peak withdrawal load.

The critical failure energy ( $G_f$ ) can be determined by the area enclosed by the load-displacement curve and the horizontal axis divided by the lateral surface area of STS,  $\pi \cdot d \cdot l$ .

Based on the test data by Khan et al. [7] and the aforementioned parameter determination procedure, the mechanical properties of the cohesive surface between STS and glulam for 8 mm and 13 mm diameter STS connections are listed in Table 3. It is worth noting that large stiffness and strength values were assigned to the  $n$  direction of cohesive surface to ensure 'hard contact', and  $s$  direction was assigned with the same parameters as  $t$  direction. Since the wood deformation along STS length direction was the main concern of this research, these assumptions had little impact on the simulation results.

**Table 3:** Mechanical properties for cohesive surface at given moisture contents.

STS	MC (%)	$\Gamma_{n,MC}$ (N/mm <sup>3</sup> )	$\Gamma_{s,MC}$ (N/mm <sup>3</sup> )	$\Gamma_{t,MC}$ (N/mm <sup>3</sup> )	$t_{n,MC}^o$ (MPa)	$t_{s,MC}^o$ (MPa)	$t_{t,MC}^o$ (MPa)	$G_{f,MC}$ (N/mm)
ASSY 8	12	500.0	19.3	19.3	100.0	16.7	16.7	91.0
	16	500.0	20.5	20.5	100.0	16.6	16.6	82.5
	21	500.0	17.3	17.3	100.0	13.8	13.8	79.4
	FSP <sup>1</sup>	500.0	15.3	15.3	100.0	10.2	10.2	50.4
VGS 13	12	500.0	9.9	9.9	100.0	16.4	16.4	128.1
	16	500.0	8.4	8.4	100.0	13.1	13.1	105.0
	21	500.0	7.6	7.6	100.0	10.3	10.3	82.0
	FSP <sup>1</sup>	500.0	7.9	7.9	100.0	10.2	10.2	83.9

Notes: <sup>1</sup> fiber saturation point, assumed as 30% in this study.

### 2.3 MODEL VERIFICATION

Apart from the specimens subjected to a constant MC before and after STS insertion, withdrawal tests were also conducted on specimens subjected to varying MC (12% - 21%, 12% - 30% and 21% - 12%) in Khan et al. [7]. In these specimens, MC of wood specimens were changed after STS installation but before STS withdrawal tests, resulting in moisture-induced stress and STS-wood relative deformation in the specimens. Based on these specimens subjected to varying MC, the numerical modelling method described in Section 2.1 was verified through comparison of the withdrawal curves from numerical modelling analysis and experimental tests by Khan et al. [7]. Fig. 2 shows examples of the comparison for 8 mm STS connections subjected to constant (model input property determination) and varying MC (model verification).

As can be seen in Fig. 2, good agreement was achieved between the FE and test withdrawal curves in terms of withdrawal stiffness, peak load and post-elastic behaviour. This indicates that the determination of STS-wood interaction properties in Section 2.2 is appropriate, and the adopted numerical modelling method in Section 2.1 is verified and can be used to predict the wetting-induced stress in STSs.

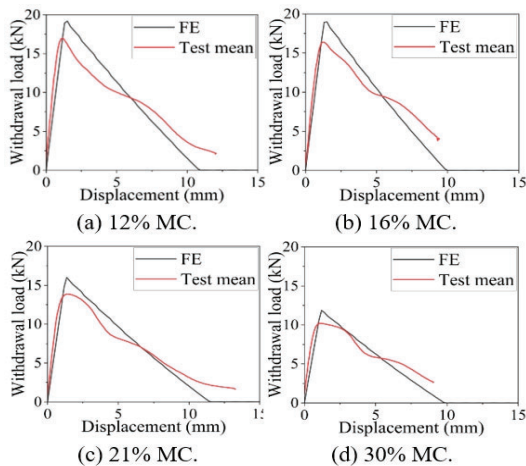


Table 4: Modelling matrix.

STS name	STS penetration length	Edge length of the specimen <sup>1</sup> (mm)	Wetting range (%)
ASSY 8	10d	25, 50, 75, 100, 125, 150, 175, 200	12 - 16, 12 - 21, 12 - 30
	20d	25, 50, 75, 100, 150, 200, 250, 300	
	30d	25, 50, 75, 100, 150, 200, 250, 300, 350, 400, 450, 500	
VGS 13	10d	25, 50, 75, 100, 150, 200, 250, 300	12 - 16, 12 - 21, 12 - 30
	20d	25, 50, 75, 100, 150, 200, 250, 300, 350, 400, 450, 500	
	30d	25, 50, 75, 100, 150, 200, 250, 300, 350, 400, 450, 500	

Notes: <sup>1</sup>  $b = h$  in Fig. 1(a).

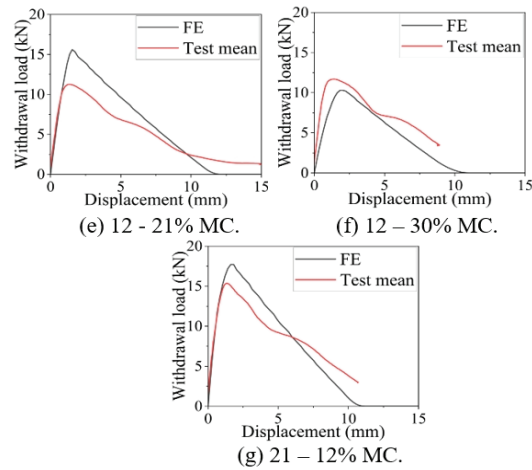


Figure 2: Comparison of withdrawal load-displacement curves of 8 mm diameter STS connections between finite element results and test results: (a) ~ (d) correspond to the specimens subjected constant MC; (e) ~ (g) correspond to the specimens subjected to varying MC.

### 2.3 MODELLING MATRIX

To investigate the specimen size effect on wetting-induced stress in STSs, three STS penetration lengths were considered in the numerical analysis: 10d, 20d and 30d. Note that due to the negligible contribution of STS tip to STS withdrawal behaviour, STS tip lengths (see Table 1) were excluded from the STS penetration lengths considered. The specimen was assumed to have a square cross-section ( $b = h$  in Fig. 1(a)). For each STS penetration length, the edge length ( $b$  and  $h$ ) of the specimen ranged from 25 mm up to 500 mm. Moreover, by assuming the MC of the wood in normal environmental condition (20 °C and 65% relative humidity) is 12%, three wetting ranges were considered: 12 - 16%, 12 - 21% and 12 - 30%. A detailed modelling matrix can be found in Table 4.

### 3 – RESULTS

#### 3.1 STRESS DISTRIBUTION IN WOOD

Due to wetting-induced wood expansion, tensile stress was developed in STSs (see Fig. 3), and wood is subjected to compressive stress along the radial direction as shown in Fig. 1(b). However, the stress distribution in wood is influenced by the specimen size. To investigate the specimen size effect on wood stress distribution along the radial direction, specimens with edge lengths of 25 mm and 100 mm were selected for comparison in Fig. 4. Both specimens were made with 8 mm diameter STSs with a penetration length of 10d and subjected to a MC increase from 12% to 16%.

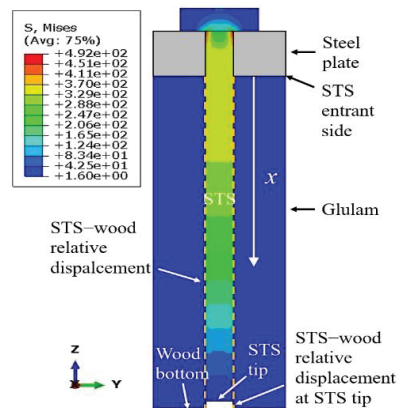


Figure 3: Wetting-induced stress in STS and STS-wood relative deformation.

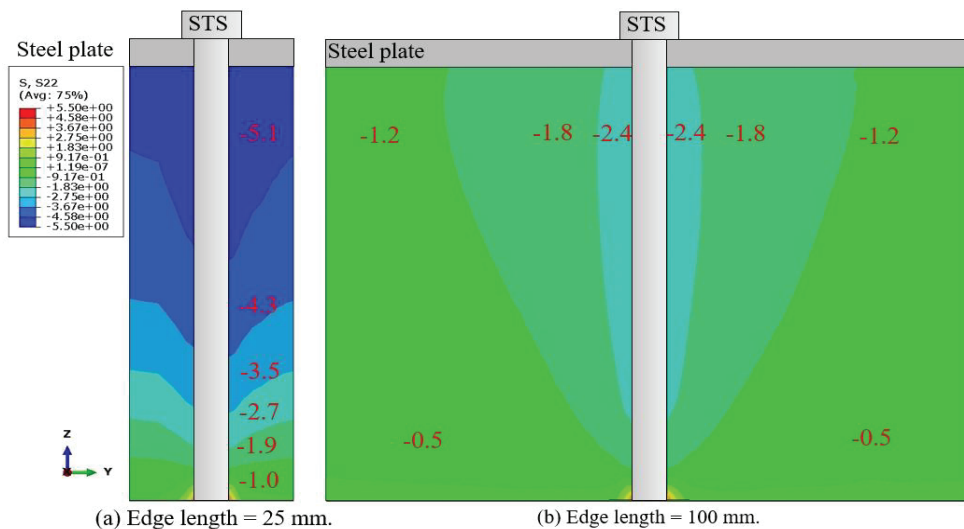


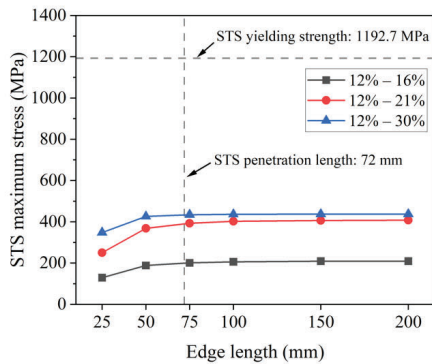
Figure 4: Wood stress distribution along radial direction for connections with 8 mm diameter STSs at 10d penetration length subjected to MC increase from 12% to 16% (cross-sectional view and units: MPa).

From Fig. 4, it is found that, for the specimen with an edge length of 25 mm, a nearly constant compressive stress (along Z direction in Fig. 4) was developed across the entire wood cross-section at the same STS penetration depth close to the screw entrant side. However, with the increase of STS penetration depth, the compressive stress in wood decreases. Smaller compressive stress was developed in wood area far away from the STS shank compared with the area near the shank of STS. For the specimen with an edge length of 100 mm, the maximum compressive stress in wood was concentrated in the area surrounding the STS shank and the compressive stress on wood at the same penetration depth varied across all cross-sections. At the cross-section close to the screw entrant side, the compressive stress decreased from 2.4 MPa near the center of the specimen to 1.2 MPa at the far end of the specimen. It is interesting to find that, in larger specimen,

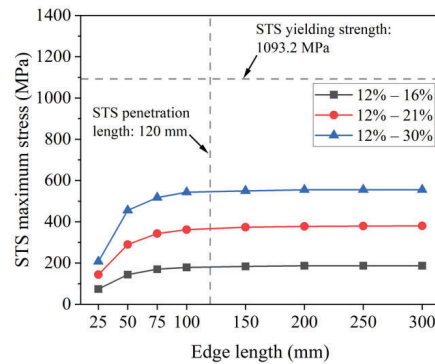
the maximum compressive stress occurred over a longer length of wood surrounding STS shank, with the stress rapidly decreasing near the tip of the STS. Moreover, smaller maximum compressive stress was developed in wood in larger specimen compared to smaller wood specimen.

#### 3.2 WETTING-INDUCED STRESS IN STS

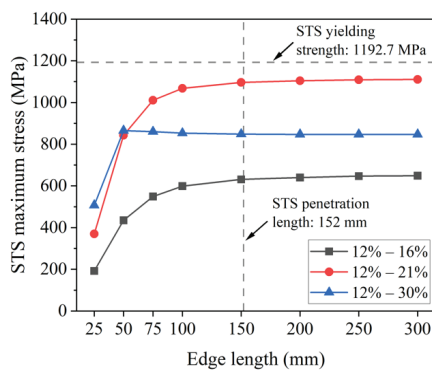
Since wetting-induced stress in STS decreases with the increase of penetration depth from STS entrant side to STS tip (see Fig. 3), in this research, only the maximum STS stress ( $x = 0$  in Fig. 3), which occurs at STS entrant side, was extracted for comparison. Results for specimens with 8 mm and 13 mm diameter STSs are summarized in Fig. 5. Note that when STS breakage occurs, the maximum STS stress is represented by yielding strength.



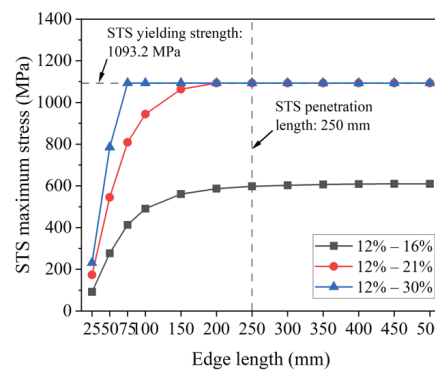
(a) 8 mm diameter STS at 10d penetration length.



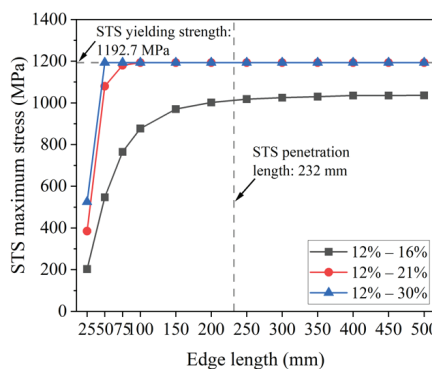
(d) 13 mm diameter STS at 10d penetration length.



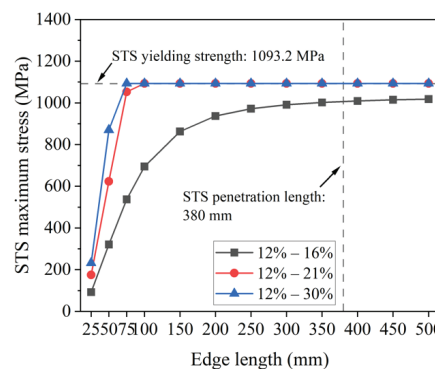
(b) 8 mm diameter STS at 20d penetration length.



(e) 13 mm diameter STS at 20d penetration length.



(c) 8 mm diameter STS at 30d penetration length.



(f) 13 mm diameter STS at 30d penetration length.

Figure 5. Wetting-induced maximum stress in STS with different specimen sizes.

It is found in Fig. 5 that, with the increase of wetting range, the maximum STS stress increases accordingly until reaching STS yielding or breakage. However, the only exception is the specimen with 8 mm diameter STS at 20d penetration length (see Fig. 5(b)), where STS stress at an MC increase from 12% to 30% were lower than those at an MC increase from 12% to 21% for specimens with edge length beyond 50 mm. This is caused by the extensive failure on cohesive surface induced by wood expansion when the relative STS-wood deformation exceeded its elastic limit,  $\delta_t^0$ , as shown in Fig. 1(d). Therefore, relative lower shear stress was

accumulated along the cohesive surface which leads to lower maximum STS stress developed for this specific case.

Generally, for all the investigated specimens, wetting-induced stress increases with the increase of specimen size when the specimen size is below 100 mm on edge length. When the specimen size is beyond 150 mm, regardless of the wetting range and STS penetration length, the maximum STS stress approaches to a constant value especially once the edge length of the specimen exceeds STS penetration length (shown as the vertical

dashed lines in Fig. 5). This indicates that, for specimens with large sizes, wetting-induced stress in wood mainly concentrates on an area with an edge length equal to STS penetration length. The contribution of wood beyond this area to the wetting-induced stress in STS is negligible. It is worth noting that the edge length of wood specimen for a single screw connection below 100 mm is not very practical. Therefore, in a real single STS steel-to-wood connection, the effect of wood specimen size on the stress development in STSs can be ignored.

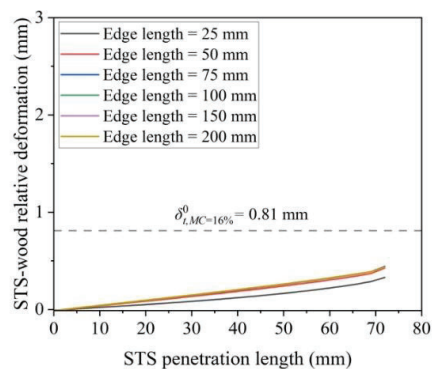
More specifically, for specimens with 10d STS penetration length, STS yielding did not occur regardless of the specimen size; for specimens with 20d STS penetration length, 13 mm diameter STS started yielding at an MC increase from 12% to 21%, and a significant STS stress increase can be seen when the edge length increases from 25 mm to 150 mm; for specimens with 30d STS penetration length, STS yielding occurred for both STS diameters at an MC increase from 12% to 21% even with a specimen edge length of 75 mm. Moreover, with an MC increase from 12% to 16%, high STS stress values close to 1000 MPa were observed in specimens with an edge length over 200 mm.

### 3.3 WETTING-INDUCED STS-WOOD RELATIVE DISPLACEMENT

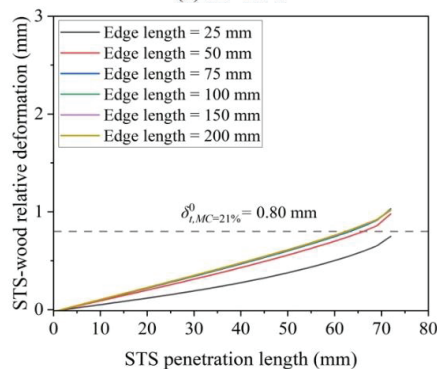
In the steel-to-wood connections, STS-wood relative deformation would occur as a result of wetting-induced wood swelling, as shown in Fig. 2. For connections subjected to large wetting range, localized withdrawal failure might occur. Since the maximum STS-wood relative deformation happens at the tip of STS, the localized withdrawal failure initiates at STS tip and propagates to STS entrant side. Therefore, by investigating the wetting-induced STS-wood relative deformation, the localised withdrawal failure propagation inside the connections was revealed. Take specimens with 8 mm diameter STSs at 10d penetration length for example, STS-wood relative deformation in different wetting conditions is summarized in Fig. 6, where the elastic limits of the STS-wood relative deformation at given MC,  $\delta_{t,MC}^0$ , are represented by the dashed horizontal lines.

It is found that STS-wood relative deformation increases along the shank of STS from the entrant side to screw tips for all the investigated connections. With MC increase from 12% to 16%, the STS-wood relative deformations of all the investigated connections are lower than the elastic limit, indicating that no damage occurred on STS-wood interaction surface. However, damage started occurring when MC increased from 12% to 21% and 30%, and with larger specimen size, damage occurred at a

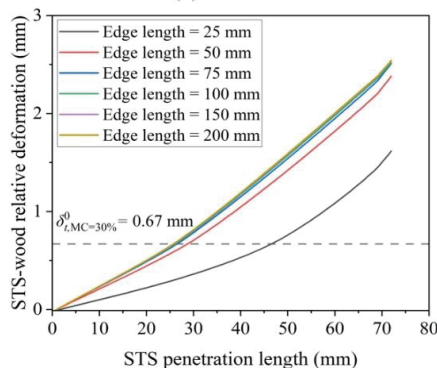
longer STS-wood interaction length. Moreover, it is observed that within a specific wetting range, increasing the specimen size from 25 mm to 50 mm results in a significant increase in STS-wood relative deformation. However, once the specimen dimension exceeds 50 mm, the increase in STS-wood relative deformation becomes negligible. Therefore, once the specimen dimension exceeds STS penetration length (72 mm in this case), which reflects the specimen size in a real single STS steel-to-wood connection, the wetting-induced STS-wood deformation remains unchanged.



(a) 12–16%.



(b) 12–21%.



(c) 12–30%.

**Figure 6:** Wetting-induced STS-wood relative deformation for specimens with 8 mm diameter STSs at 10d penetration length with different specimen sizes.

## 4 – CONCLUSIONS

In this study, the effect of specimen sizes on wetting-induced failure of steel-to-wood STS connections was investigated through numerical modelling analysis via ABAQUS. By incorporating STSs of different diameters (8 mm and 13 mm) and different STS penetration lengths (10d, 20d and 30d), the main study findings are summarized as follows:

- The specimen size does have a significant impact on the wetting-induced STS stress and STS-wood relative displacement when the specimen size is below 100 mm on edge length. In this case, with the increase of specimen size, both wetting-induced STS stress and STS-wood relative displacement increase at a given wetting range.
- The effect of specimen size remains unchanged when the specimen size exceeds STS penetration length, resulting in negligible increase in wetting-induced STS stress and STS-wood relative displacement. The wood specimen size in a real single STS steel-to-wood connection is usually larger than 100 mm and belongs to this category. Therefore, the effect of wood specimen size to the stress development in STSs can be ignored in a real single STS connection.

## 5 – Future study

This research investigated the effect of specimen size on performance of single-STs connections. Further study considering a group of screws connections with different screw spacing will be conducted in the next phase research.

## 6 – ACKNOWLEDGEMENT

The authors would like to thank BC Forestry Innovation Investment Ltd. for funding support of this research (Project # 24/25-UVIC-MCE-W25-050).

## 7 – REFERENCES

- [1] Pirnbacher G. Beanspruchungs-und Optimierungs-potentiale selbstbohrender Holzschrauben. 15 Internationale Holzbau-Forum. Graz, Österreich, vol. 1, 2009, p. 1.
- [2] Ringhofer A, Grabner M, Silva C, Branco J, Schickhofer G. The influence of moisture content variation on the withdrawal capacity of self-tapping screws. *Holztechnologie* 2014;55:33–40.
- [3] Silva C, Branco JM, Ringhofer A, Lourenço PB, Schickhofer G. The influences of moisture content variation, number and width of gaps on the withdrawal resistance of self tapping screws inserted in cross laminated timber. *Construction and Building Materials* 2016;125:1205–15. <https://doi.org/10.1016/j.conbuildmat.2016.09.008>.
- [4] Gutknecht MP, MacDougall C. Withdrawal resistance of structural self-tapping screws parallel-to-grain in common Canadian timber species. *Can J Civ Eng* 2019;46:952–62. <https://doi.org/10.1139/cjce-2018-0374>.
- [5] Gerstorfer D, Forte T, Füssl J. Experimental and numerical determination of the screw deformation in laminated beech veneer lumber as a result of moisture-induced swelling. *Civil Engineering Design* 2021;3:171–8.
- [6] Khan MT, Ni C, Wang J, Chui YH. Numerical Investigation of the Axial Stress Distribution of Self-Tapping Screws in Mass Timber Products during Wetting or Drying. *Buildings* 2023;13:623. <https://doi.org/10.3390/buildings13030623>.
- [7] Khan MT, Ni C. Expanding wood use towards 2025. Developing design guidelines to prevent failure of self-tapping screw due to wetting, year 2. 2022.
- [8] MatWeb. Search engineering material by property value. 2023. <https://www.matweb.com> (accessed November 2, 2023).
- [9] Ross RJ. Wood handbook: Wood as an engineering material. Madison, WI, USA: U.S. Department of Agriculture, Forest Service, Forest Products Laboratory; 2021.
- [10] Jensen JL, Koizumi A, Sasaki T, Tamura Y, Iijima Y. Axially loaded glued-in hardwood dowels. *Wood Science and Technology* 2001;35:73–83. <https://doi.org/10.1007/s002260000076>.